Chinese Journal of Natural Medicines

***Hypericum monogynum* extract inhibits human aortic valve interstitial cell calcification by interfering with the EGFR/PI3K/AKT signaling pathway**

Zhengfeng Fan, Jincheng Hou, Jiangchun Wei, Pengning Fan, Fuqiang Tong, Shiqi Chen, Lin Fan, Xingyu Qian, Bingchuan Geng, Chen Jiang, Yixuan Wang, Pingping Fan, Yahui Huang, Fei Li, Yonghui Zhang, Zhengxi Hu, Nianguo Dong

Citation: Zhengfeng Fan, Jincheng Hou, Jiangchun Wei, Pengning Fan, Fuqiang Tong, Shiqi Chen, Lin Fan, Xingyu Qian, Bingchuan Geng, Chen Jiang, Yixuan Wang, Pingping Fan, Yahui Huang, Fei Li, Yonghui Zhang, Zhengxi Hu, Nianguo Dong, *Hypericum monogynum* extract inhibits human aortic valve interstitial cell calcification by interfering with the EGFR/PI3K/AKT signaling pathway, Chinese Journal of Natural Medicines, 2026, 24(4), 402–413. doi: 10.1016/S1875–5364(26)61170–3.

View online: https://doi.org/10.1016/S1875–5364(26)61170–3

Related articles that may interest you

Jiedu Sangen decoction inhibits chemoresistance to 5–fluorouracil of colorectal cancer cells by suppressing glycolysis *via* PI3K/AKT/HIF–1 α signaling pathway

Chinese Journal of Natural Medicines. 2021, 19(2), 143–152 https://doi.org/10.1016/S1875–5364(21)60015–8

Scutellaria baicalensis: a promising natural source of antiviral compounds for the treatment of viral diseases

Chinese Journal of Natural Medicines. 2023, 21(8), 563–575 https://doi.org/10.1016/S1875–5364(23)60401–7

The bioinformatics and metabolomics research on anti–hypoxic molecular mechanisms of Salidroside *via* regulating the PTEN mediated PI3K/Akt/NF– κ B signaling pathway

Chinese Journal of Natural Medicines. 2021, 19(6), 442–453 https://doi.org/10.1016/S1875–5364(21)60043–2

The combination of EGCG with warfarin reduces deep vein thrombosis in rabbits through modulating HIF–1 α and VEGF *via* the PI3K/AKT and ERK1/2 signaling pathways

Chinese Journal of Natural Medicines. 2022, 20(9), 679–690 https://doi.org/10.1016/S1875–5364(22)60172–9

Screening of the ubiquitin–proteasome system activators for anti–Alzheimer’s disease by the high–content fluorescence imaging system

Chinese Journal of Natural Medicines. 2022, 20(1), 33–42 https://doi.org/10.1016/S1875–5364(22)60152–3

EGCG and ECG induce apoptosis and decrease autophagy *via* the AMPK/mTOR and PI3K/AKT/mTOR pathway in human melanoma cells

Chinese Journal of Natural Medicines. 2022, 20(4), 290–300 https://doi.org/10.1016/S1875–5364(22)60166–3

Wechat

Chinese Journal of Natural Medicines 24 (2026) 402-413

Contents lists available at ScienceDirect

Chinese Journal of Natural Medicines

journal homepage: www.cjnmcpu.com/

Original article

Hypericum monogynum extract inhibits human aortic valve interstitial cell calcification by interfering with the EGFR/PI3K/AKT signaling pathway

Zhengfeng Fan[a,Δ], Jincheng Hou[a,Δ], Jiangchun Wei[b,Δ], Pengning Fan[a], Fuqiang Tong[a], Shiqi Chen[a], Lin Fan[a], Xingyu Qian[a], Bingchuan Geng[a], Chen Jiang[a], Yixuan Wang[a], Pingping Fan[b], Yahui Huang[b], Fei Li[a,*], Yonghui Zhang[b,*], Zhengxi Hu[b,c,*], Nianguo Dong[a,*]

[a] *Department of Cardiovascular Surgery, Union Hospital, Tongji Medical College, Huazhong University of Science and Technology, Wuhan 430022, China*
[b] *Hubei Key Laboratory of Natural Medicinal Chemistry and Resource Evaluation, and Wuhan (China-Romania) Belt and Road Joint Laboratory on Traditional Chinese Medicine, School of Pharmacy, Tongji Medical College, Huazhong University of Science and Technology, Wuhan 430030, China*
[c] *Hubei Shizhen Laboratory, Wuhan 430061, China*

ARTICLE INFO

Article history:
Received 12 March 2025
Revised 5 June 2025
Accepted 12 June 2025
Available online 20 April 2026

Keywords:
Hypericum monogynum
Calcific aortic valve disease
Drug screening
Dot-blotting
Natural compound
EGFR

ABSTRACT

Calcific aortic valve disease (CAVD) is a serious heart valve condition with increasing global prevalence. Currently, transcatheter aortic valve implantation (TAVI) or surgical aortic valve replacement (SAVR) represents the only available treatment strategy, as no pharmaceutical therapies for CAVD are approved. The aim of this study was to identify compounds capable of inhibiting osteogenic differentiation of human aortic valve interstitial cells (hVICs), a process critically implicated in CAVD pathogenesis, and to elucidate the underlying molecular mechanism. From an in-house library of 88 compounds screened *via* dot-blotting, we identified chipericumin D, a natural compound extracted from *Hypericum monogynum* L., as a candidate exhibiting potent inhibitory activity against hVIC osteogenic differentiation. Network pharmacology analysis, molecular docking, drug affinity responsive target stability (DARTS), cellular thermal shift assay (CETSA), and surface plasmon resonance (SPR) collectively demonstrated direct binding of chipericumin D to the epidermal growth factor receptor (EGFR). Furthermore, chipericumin D suppressed activation of the EGFR/phosphatidylinositol 3-kinase (PI3K)/protein kinase B (AKT) signaling pathway in hVICs cultured under osteogenic medium (OM) conditions. These findings indicate that chipericumin D is a promising therapeutic candidate for CAVD, and provide preliminary evidence that EGFR constitutes a novel molecular target for CAVD intervention.

1. Introduction

Calcific aortic valve disease (CAVD) is a serious heart valve condition associated with substantial global prevalence and mortality [1]. According to the Global Burden of Disease database, the prevalence of CAVD was 9.4 million in 2019 [2]. Currently, transcatheter aortic valve implantation (TAVI) or surgical aortic valve replacement (SAVR) represents the only available treatment strategy for CAVD [3]. However, surgical interventions are associated with high risks [4], numerous complications [5], substantial costs, and a reduced postoperative quality of life [6]. Although clinical trials of statin drugs have demonstrated their ability to lower serum lipoprotein(a) levels, they fail to reverse CAVD progression [7]. Therefore, the identification of pharmacological agents capable of delaying CAVD progression remains an urgent clinical need.

The aortic valve cusps predominantly consist of valve interstitial cells (VICs) and valve endothelial cells (VECs). Numerous studies have shown that CAVD pathogenesis involves endothelial injury [8], lipid deposition, and inflammatory responses, followed by pathological osteogenic differentiation of VICs [9,10], which is believed to play a crucial role in CAVD development [11]. This process leads to collagen deposition, extracellular matrix (ECM) remodeling, and nucleation site formation [12], accompanied by up-regulation of osteogenic-specific genes such as alkaline phosphatase (ALP) and RUNX2 [13]. Consequently, identifying drugs that inhibit VIC osteogenic differentiation constitutes a promising therapeutic strategy for CAVD.

Current high-content drug screening approaches are primarily based on either disease target-focused virtual screening [14] or disease phenotype-based screening [15]. For instance, a comprehensive virtual drug screen leveraging a broad gene network in human disease-relevant iPSC-derived cells identified XCT790 as a compound effective in both preventing and treating CAVD in a mouse model [14]. Similarly, phenotype-based screening combined with deep learning identified TYA-018, a highly selective HDAC6 inhibitor, as a candidate for treating dilated cardiomyopathy

* Corresponding author.
E-mail addresses: lifei_union@hust.edu.cn (F. Li); zhangyh@mails.tjmu.edu.cn (Y. Zhang); hzx616@126.com (Z. Hu); 1986xh0694@hust.edu.cn (N. Dong)
[Δ] These authors contributed equally to this work.

https://doi.org/10.1016/S1875-5364(26)61170-3

(DCM) [15]. Nevertheless, large-scale drug screening studies specifically targeting CAVD phenotypes have not yet been reported.

The aim of this study was to screen compounds based on the VIC osteogenic differentiation phenotype and to explore the underlying mechanisms of drug action in CAVD.

2. Materials and methods

2.1. Reagents and antibodies

Supporting information lists the main reagents and antibodies used in this study.

2.2. Cell culture and stimulation

As described in previous studies [16], aortic valves were digested with 2 mg·mL^{-1} type I collagenase at 37 °C for 10 h. The isolated cells were cultured in complete medium consisting of high-glucose (HG, 4.5 g·L^{-1} D-glucose) Dulbecco's modified Eagle's medium (DMEM, Gibco, Invitrogen, Carlsbad, CA, USA), 1% streptomycin-penicillin, and 10% fetal bovine serum (FBS). Human VICs (hVICs) at passages 3 to 5 were used for subsequent experiments. Osteogenic differentiation was induced using osteogenic medium (OM) containing DMEM, 2% FBS, 100 nmol·L^{-1} dexamethasone, 50 μg·mL^{-1} L-ascorbic acid, and 10 mmol·L^{-1} β-glycerophosphate. Unless otherwise specified, cells were treated with OM or test compounds for 3 days for Western blotting, 7 days for ALP staining, and 21 days for Alizarin Red (AR) staining. All screened compounds were provided by the School of Pharmacy, Tongji Medical College, Huazhong University of Science and Technology.

2.3. Cell viability analysis

As previously described [17], cells were seeded in 96-well plates and treated with various concentrations (0.1, 0.3, 0.5, 1, 3, 5, 10, 30, 50, and 100 μmol·L^{-1}) of each compound for 72 h. Subsequently, cells were incubated with DMEM containing 10% CCK-8 reagent at 37 °C for 2 h, and absorbance was measured at 450 nm using a microplate reader (Thermo Fisher Scientific). The half maximal inhibitory concentration (IC_{50}) values were calculated using GraphPad Prism 10.0 software.

2.4. Quantitative real-time polymerase chain reaction (qRT-PCR) assay

Total ribonucleic acid (RNA) was extracted from hVICs using an RNA extraction kit (TIANGEN, A0508A) and reverse-transcribed into complementary deoxyribonucleic acid (cDNA) using HiScript III RT SuperMix (Vazyme, R323-01). qRT-PCR was performed on a Step One Plus thermal cycler using SYBR Green (Vazyme, 7E782J3) according to the manufacturer's instructions, with β-actin serving as the internal control. Relative gene expression was analyzed using the ΔΔCt method. Primer sequences are provided in Supplementary Table S1.

2.5. Western blotting analysis

As previously reported [17], cultured cells were lysed on ice in radioimmunoprecipitation assay (RIPA) buffer (Beyotime, P0013K) supplemented with 1% protease and phosphatase inhibitors. Lysates were sonicated and centrifuged, and protein concentrations were determined using a bicinchoninic acid (BCA) assay kit (Beyotime, P0011). Equal amounts of protein were separated by 4%–20% sodium dodecyl sulfate polyacrylamide gel electrophoresis (SDS-PAGE, ACE Biotechnology, ET15412Gel) and transferred onto polyvinylidene fluoride (PVDF) membranes (Millipore, 03010040001). Membranes were incubated overnight at 4 °C with primary antibodies, followed by 1 h incubation with appropriate secondary antibodies at room temperature. Immunoreactive bands were visualized using an enhanced chemiluminescence (ECL) kit (HYCEZMBIO, HYC0316) and quantified using ImageJ software (NIH).

2.6. Dot-blotting analysis

VICs treated under different conditions for 72 h were lysed on ice in RIPA buffer containing 1% protease/phosphatase inhibitors for 10 min. Protein extracts were then dotted onto nitrocellulose (NC) membranes and air-dried at 37 °C for 10 min to fix the proteins. Membranes were blocked at room temperature for 1 h, incubated overnight at 4 °C with specific primary antibodies, and subsequently incubated for 1 h at room temperature with appropriate secondary antibodies. Immunoreactivity was detected using an ECL kit per the manufacturer's instructions, and signal intensities were analyzed using ImageJ software (NIH).

2.7. Immuno-fluorescent staining assays

VICs were subjected to immunofluorescent staining following standard protocols from prior studies [17]. After 3 days of treatment, the cells were fixed with 4% paraformaldehyde (PFA) for 10 min, permeabilized, and blocked with QuickBlock™ Blocking Buffer for Immunostaining (Beyotime, P0260) for 15 min. The cells were then incubated overnight at 4 °C with specific primary antibodies, followed by incubation with the corresponding fluorescent secondary antibodies for 1 h at room temperature in the dark. Images were acquired using a fluorescence microscope and semi-quantitatively analyzed with ImageJ software (NIH).

2.8. ALP staining assays

Following the manufacturer's instructions, cells treated for 7 days were fixed with 4% PFA for 10 min and incubated in the dark with BCIP/NBT Alkaline Phosphatase Color Development Kit (Beyotime, C3206) for 15 min. Images were captured using an optical microscope (Mshot). ALP-positive cells appeared as deep blue/purple, and stained areas were quantified using ImageJ software (NIH).

2.9. AR staining assays

AR staining was used to assess calcification, with stained areas reflecting calcification levels. After 21 days of treatment, cells were fixed with 4% PFA for 10 min and incubated with AR staining reagent (Servicebio, G1038) for 10 min, following the manufacturer's protocol. Images were acquired using an optical microscope (Mshot) and analyzed with ImageJ software (NIH).

2.10. Prediction of potential compound targets

The SMILES structure of chipericumin D was retrieved from the PubChem database (https://pubchem.ncbi.nlm.nih.gov/). Potential targets were predicted using the SEA database (https://sea.bkslab.org/), the Swiss Target Prediction (STP) database (http://swisstargetprediction.ch/), and the Super-PRED database (https://prediction.charite.de/). Additionally, chipericumin D was screened against a pharmacophore library [18]. Following initial screening, targets were further filtered based on fitness scores and manual curation, as detailed in Supplementary Table S2.

2.11. Acquisition of CAVD target genes

Human genes associated with CAVD were retrieved from the DisGeNET database (https://www.disgenet.com/), GeneCards

database (https://www.genecards.org/), and the National Center for Biotechnology Information (NCBI) database (https://www.ncbi.nlm.nih.gov/) using the keyword "calcific aortic valve disease." Genes from these sources were consolidated, and duplicates were removed to generate a non-redundant set of CAVD-related target genes (Supplementary Table S2).

2.12. The PPI network of chipericumin D and CAVD overlapping targets

The STRING database (https://cn.string-db.org/) was used to construct a protein-protein interaction (PPI) network of overlapping target genes. Node size and color intensity were adjusted according to degree values in the PPI network, with larger and darker nodes representing higher connectivity.

2.13. Gene Ontology (GO) and Kyoto Encyclopedia of Genes and Genomes (KEGG) pathway enrichment analysis

Overlapping target genes underwent GO and KEGG pathway enrichment analyses. Pathways and GO terms with adjusted *P*-values < 0.05 were considered significant and were obtained using the STRING database (Supplementary Table S3). Bubble plots were generated for visualization using R 4.4.0 software.

2.14. Molecular docking

As previously described [17], protein crystal structures were obtained from the Protein Data Bank (PDB) (Table 2). Molecular docking was performed using AutoDock Vina. Receptor proteins were prepared in PyMOL by removing salt ions, water molecules, and co-crystallized ligands. The docking box was defined, and ADFRsuite was used to convert preprocessed small molecules and receptors into the PDBQT format required for AutoDock Vina. The global search exhaustiveness was set to 32, with all other parameters at default values. Docking results were visualized using PyMOL.

2.15. Drug affinity responsive target stability (DARTS) analysis

As previously reported [19], DARTS is a key method for identifying or validating targets of small -molecule compounds. Briefly, protein extracts from hVICs were quantified using the BCA method. Chipericumin D was incubated with the protein lysate at room temperature for 1 h, followed by digestion with pronase E for 10 min. Target protein stability was then assessed by Western blotting.

2.16. Cellular thermal shift assay (CETSA) analysis

The CETSA experiment was performed as previously described [20]. hVICs were treated with chipericumin D (3 μmol·L^{-1}) or DMSO for 24 h and harvested in PBS containing protease and phosphatase inhibitors. Lysates were divided into six aliquots and heated for 5 min at temperatures ranging from 42 to 67 °C in a thermal cycler, then cooled at room temperature for 3 min. After three freeze-thaw cycles in liquid nitrogen and centrifugation at 13,000 × *g* for 15 min, samples were mixed with loading buffer, heated at 100 °C for 7 min, and analyzed by Western blotting.

2.17. Surface plasmon resonance (SPR) analysis

SPR is a label-free, real-time optical technique used to study interactions between small molecules and proteins [21]. SPR provides insights into molecular affinity and kinetics by determining binding parameters, including the dissociation constant (K_D), association rate constant (K_a), and dissociation rate constant (K_d) [22]. Human epidermal growth factor receptor (EGFR) was covalently immobilized on a CM5 sensor chip *via* amine coupling: the chip was activated with a mixture of 1-ethyl-3-(3-dimethylaminopropyl)-carbodiimide (EDC, GE Healthcare) and *N*-hydroxysuccinimide (NHS, GE Healthcare), followed by injection of EGFR solution and blocking with ethanolamine. In total, 12,030 resonance units (RU) of human EGFR protein were immobilized (Fig. S4). Binding kinetics and affinity between chipericumin D and EGFR were analyzed using a Biacore system (GE Healthcare). Data were globally fitted to the Langmuir binding model using Biacore Insight Evaluation software (Cytiva, Marlborough, MA, USA) to derive binding and dissociation constants.

2.18. Statistical analysis

Data are presented as mean ± SD and were analyzed using two-tailed unpaired Student's *t*-test or one-way ANOVA in GraphPad Prism 10.0 software. Statistical significance was defined as $^{*}P < 0.05$.

3. Results

3.1. Eighty-eight compound library screening in human VICs for anti-calcification

To validate the 96-well plate dot-blotting assay, hVIC calcification was induced using OM (see Fig. S1 for VIC phenotyping), and time-dependent changes in RUNX2 expression were assessed by both dot-blotting and Western blotting (Fig. 1A). Notably, RUNX2 protein expression increased significantly over time in both assays (Figs. 1B and 1C).

Based on this validation, we performed a drug screen targeting hVIC osteogenic differentiation using dot-blotting, as outlined in the screening workflow (Fig. 1D). Each 96-well plate included negative controls (normal culture medium) and positive controls (OM). Eighty-eight compounds were tested at a concentration of 4 μmol·L^{-1} (Fig. 1E). RUNX2 expression in the four positive control wells (OM, lower left corner) was significantly higher than in the four negative control wells (CTR, upper left corner) (Figs. 1E and 1F). The relative fold change of RUNX2 protein expression in OM-treated wells was 1.80 compared to the CTR group (Table 1). The top 10 candidate compounds reduced RUNX2 expression to levels ranging from 1.19- to 1.29-fold over control (Fig. 1G and Table 1). These top candidates were subsequently evaluated to identify the most effective compound.

3.2. Chipericumin D exhibits relatively superior anti-calcification activity

We performed AR staining to further quantify anti-calcification activity in 12-well plates (Fig. 2A). Compounds **61**, **49**, and **82** significantly reduced calcium deposits in hVICs (Fig. 2B). ALP staining results indicated that compounds **61**, **49**, **82**, **27**, **51**, **59**, **6** and **48** significantly inhibited ALP activity compared to the OM group (Figs. 2A and 2C). Western blotting results showed that, except for compounds **6** and **48**, the remaining eight compounds significantly reduced ALP protein expression (Figs. 2D and 2E). Moreover, all ten candidate compounds significantly suppressed RUNX2 protein expression (Figs. 2D and 2F), consistent with the dot-blotting results in Fig. 1 (Fig. 2F). Collectively, these findings suggest that compounds **61**, **49**, and **82** may inhibit osteogenic differentiation of hVICs. Considering compound availability and purification complexity, we selected compound **82** for subsequent experiments. The molecular structure of compound **82** has been identified (Fig. 2G), and the compound was characterized as chipericumin D [23] and isolated from *Hypericum monogynum* L.

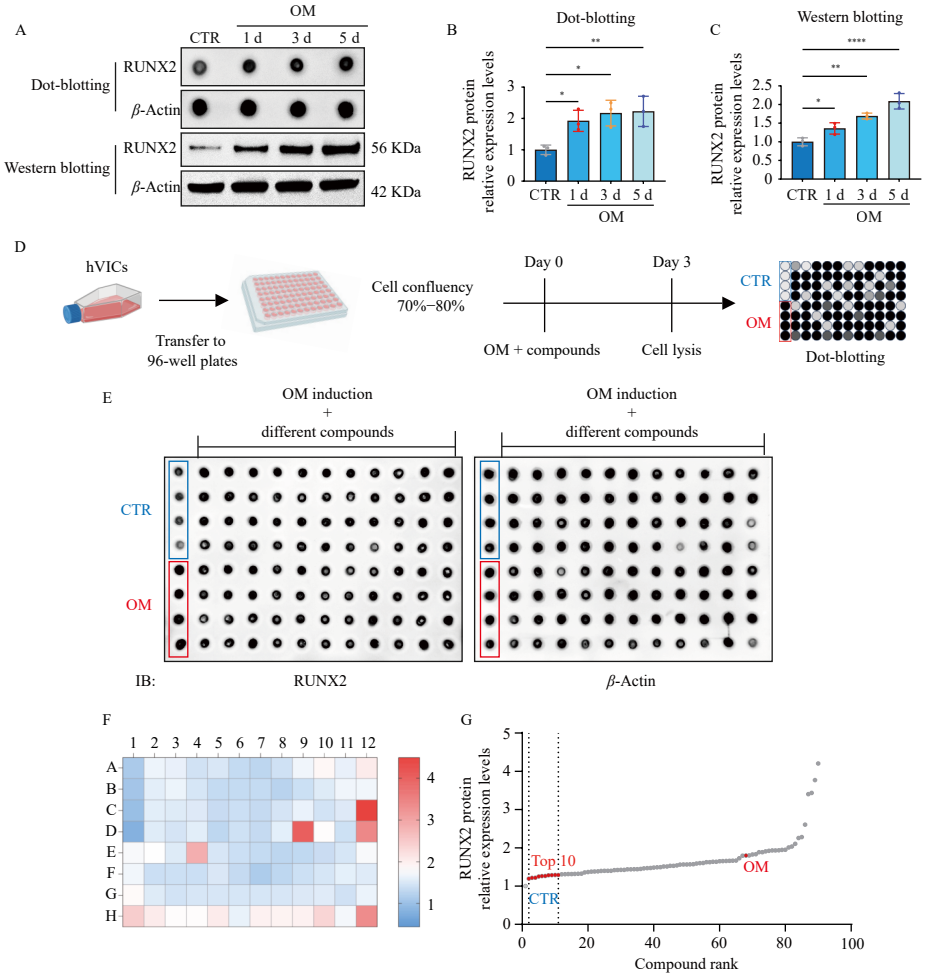

Fig. 1 Screening of an 88-compound library for anti-calcification effects in human VICs. (A–C) RUNX2, a calcification-related protein, was measured in hVICs cultured in osteogenic medium (OM) for 1, 3, or 5 days by dot blotting and Western blotting. CTR denotes the control group, and OM denotes the osteogenic medium group. $^{*}P < 0.05$ was considered statistically significant compared with CTR; $^{**}P < 0.01$, $^{****}P < 0.0001$. (D) Workflow of the compound screening process. (E) Representative dot blotting results of RUNX2 and β-actin protein expression. (F) Heat-map of RUNX2/β-actin ratio derived from (E). (G) Scatter plot of RUNX2 protein expression derived from (E). Data are presented as means ± SD ($n = 3$).

Table 1 The top 10 candidate compounds reduced RUNX2 expression.

Compound rank	Compound number	RUNX2 protei n relative expression levels
CTR	—	1.00
OM	—	1.80
1	**28**	1.19
2	**37**	1.22
3	**61**	1.22
4	**49**	1.25
5	**82**	1.26
6	**27**	1.27
7	**51**	1.28
8	**59**	1.29
9	**6**	1.29
10	**48**	1.29

CTR means control, OM means osteogenic medium, "Compound number" means different compound, and "—" means no data.

During the purification of *Hypericum monogynum*, we isolated an additional 11 compounds, four of which are novel natural products (see Supporting Information). The pharmacological properties of these new natural compounds warrant further investigation to fully elucidate their potential biological effects. In the following sections, we explore the pharmacological effects of chipericumin D in CAVD.

Table 2 The docking scores for the binding of chipericumin D with EGFR, NF-κB1, TLR4, STAT3, and HIF1A.

Target name	PDB ID	Docking score (kcal·mol^{-1})
EGFR	2RGP	−7.265
NF-κB1	3GUT	−6.313
TLR4	3FXI	−6.264
STAT3	6NJS	−6.032
HIF1A	4H6J	−5.605

3.3. Effect of chipericumin D on cell viability

The IC_{50} of chipericumin D in human epidermoid carcinoma KB cells and murine lymphoma L1210 cells exceeds 10 μg·mL^{-1} *in vitro* [23]. To assess cytotoxicity against hVICs, we determined the IC_{50}, which was approximately 27.57 μmol·L^{-1} (Fig. 3A).

3.4. Chipericumin D inhibits hVIC osteogenic differentiation in vitro

We used Western blotting to determine the optimal concen-

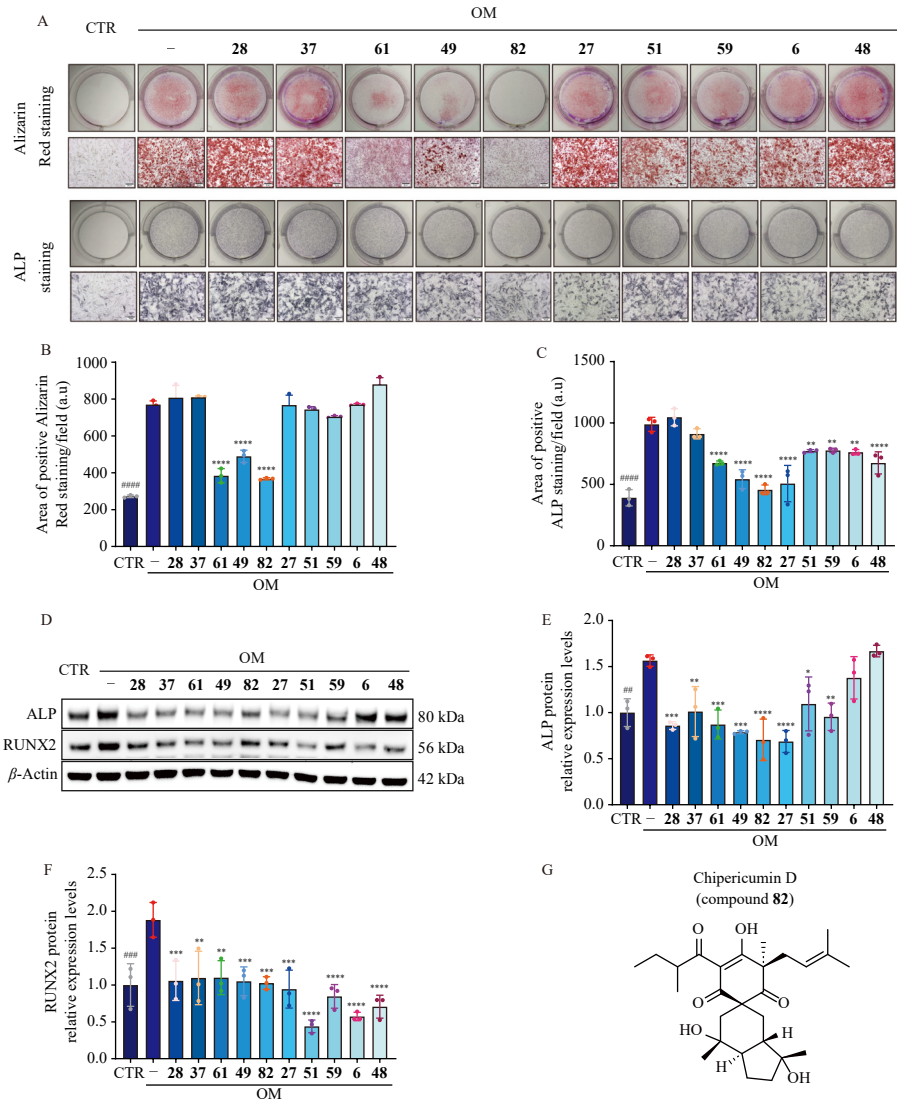

Fig. 2 Chipericumin D exhibits relatively potent anti-calcification activity. (A–C) Alizarin Red staining and ALP staining of hVICs cultured under different conditions. (D–F) ALP and RUNX2 protein expression in hVICs cultured under different conditions. OM + number denotes OM treatment in the presence of different compounds. "#" indicates comparison between CTR and OM, whereas "*" means comparison between OM + number and OM. $^{*}P < 0.05$ and $^{\#}P < 0.05$ were considered statistically significant; $^{**}P < 0.01$, $^{***}P < 0.001$, ****, $^{\#\#\#\#}P < 0.0001$. (G) Molecular structure of chipericumin D (compound **82**). Data are presented as means ± SD ($n = 3$).

tration of chipericumin D for suppressing ALP and RUNX2 protein expression in hVICs under OM induction (Figs. 3B–3D). Chipericumin D was effective at concentrations above 1 μmol·L^{-1}.

Subsequently, hVICs were cultured in OM with or without 3 μmol·L^{-1} chipericumin D. Although chipericumin D exhibits cytotoxicity, cell viability was comparable at 1 and 3 μmol·L^{-1}, with a more pronounced inhibitory effect observed at the higher concentration. After 3 days of culture, hVIC morphology differed between OM-treated and chipericumin D-treated groups (Fig. S2). Compared with the control (CTR) group, the OM group induced disordered cell orientation, whereas chipericumin D treatment restored consistent alignment. Gene expression levels of *ALP* and *RUNX2* were significantly down-regulated by chipericumin D relative to the OM group (Figs. 3E and 3F). Protein expression levels of ALP and RUNX2 aligned with the gene expression data (Figs. 3G–3I). Immunofluorescence (IF) staining revealed differential RUNX2 expression and nuclear import ratios between the OM and OM + chipericumin D groups (Figs. 3J and 3K). AR staining demonstrated a significant reduction in calcification upon chipericumin D treatment (Figs. 3L and 3M). Additionally, ALP activity in hVICs decreased significantly with chipericumin D (Figs. 3N and 3O), consistent with the aforementioned findings.

3.5. Network pharmacology analysis identifies the potential target of chipericumin D

First, we predicted potential targets of chipericumin D, retrieving 138 targets from the STP, SEA, and Super-PRED databases, and 24 from the pharmacophore database. After removing duplicates, we obtained 155 unique targets (Fig. 4A and Table S2).

Second, using "calcific aortic valve disease" as a keyword, we identified 1586, 51, and 27 CAVD-associated target genes from the NCBI, GeneCards, and DisGeNET databases, respectively. Merging and deduplicating these yielded 1609 CAVD-related genes (Fig. 4A and Table S2).

We then generated a Venn diagram illustrating the intersection of chipericumin D and CAVD targets (Fig. 4A). To elucidate the complex interactions among chipericumin D, CAVD, and their targets, we constructed a chipericumin D-CAVD-targets network (Fig. 4B). Furthermore, we built a PPI network of overlapping targets using the STRING database, which comprised 30 nodes and 129 edges (Fig. 4C). Visualization in Cytoscape 3.9.1 revealed that signal transducer and activator of transcription 3 (STAT3), EGFR, NF-κB1, hypoxia-inducible factor 1A (HIF1A), and Toll-like receptor 4 (TLR4) were the top five nodes by degree (Fig. 4C).

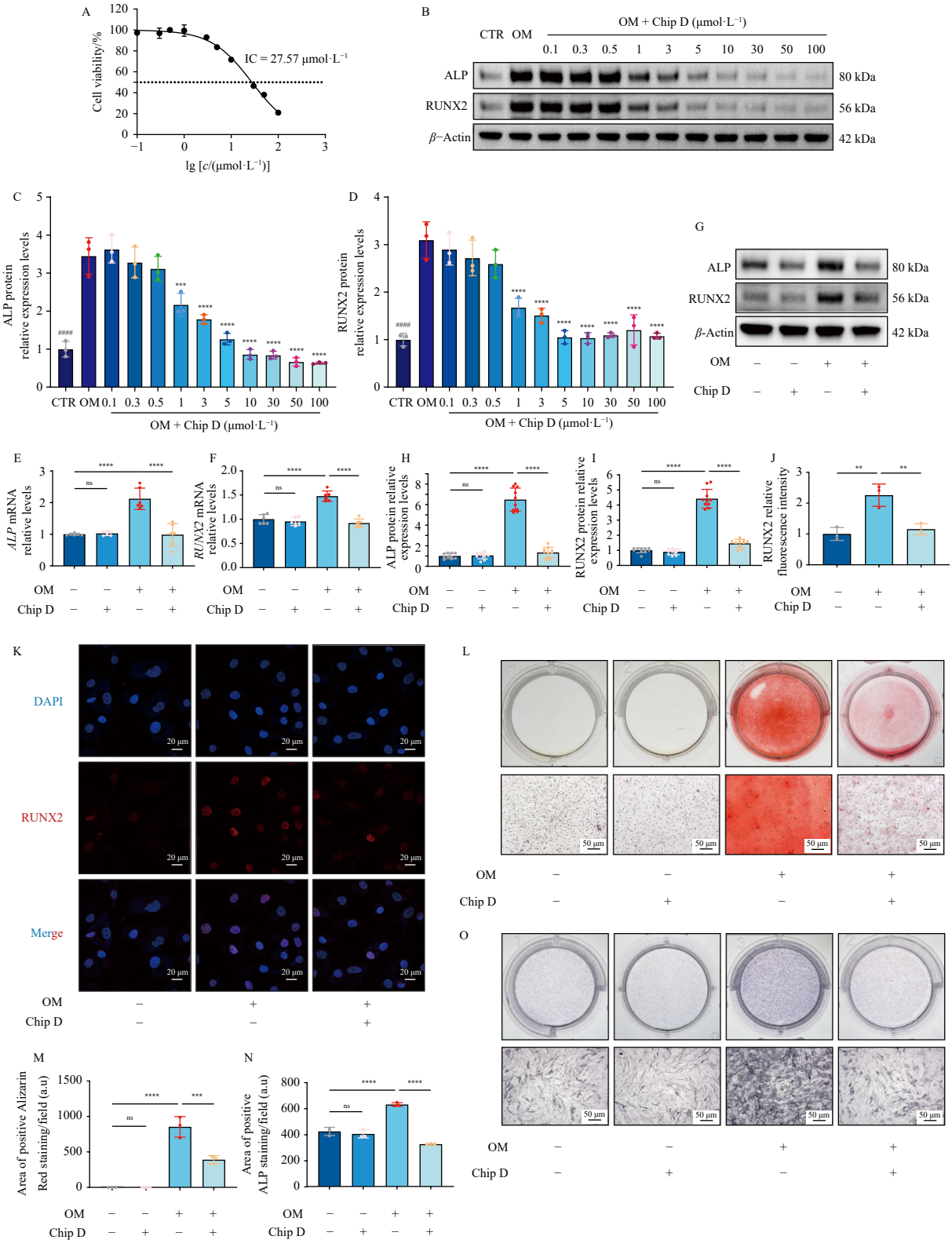

Fig. 3 Chipericumin D inhibits OM-induced osteogenic differentiation in hVICs *in vitro*. (A) Half-maximal inhibitory concentration (IC_{50}) of chipericumin D (Chip D) in hVICs. Chip D concentrations were log-transformed. n = 3. (B–D) Western blotting analysis of hVICs treated with different concentrations of Chip D. n = 3. "#" comparison between CTR and OM, whereas "*" indicates comparison between OM + Chip D (different concentrations) and OM. $^{*}P < 0.05$ and $^{\#}P < 0.05$ were considered statistically significant; $^{***}P < 0.001$, ****, $^{\#\#\#\#}P < 0.0001$. (E–F) *ALP* and *RUNX2* gene levels under different treatments. n = 6. (G–I) Western blotting analysis of hVICs under different treatments. n = 10. (J–K) Immunofluorescence staining of RUNX2. n = 3 (scale bar: 20 μm). (L–M) Alizarin Red staining. n = 3. (N–O) ALP staining. n = 3. The Chip D (3 μmol·L^{-1}) was used for treatment. Data are presented as means ± SD.

Finally, we selected these top five proteins for molecular docking analysis. Chipericumin D interacted with EGFR, NF-κB1, TLR4, STAT3, and HIF1A *via* multiple amino acid residues (Figs. 4D–4H). Lower docking scores indicate stronger binding affinity. Chipericumin D exhibited the highest affinity for EGFR (−7.265 kcal·mol^{-1}) and the lowest for HIF1A (−5.605 kcal·mol^{-1}) (Table 2). Hydrogen bonding between chipericumin D and its targets enhanced binding stability, while hydrophobic interactions at mul-

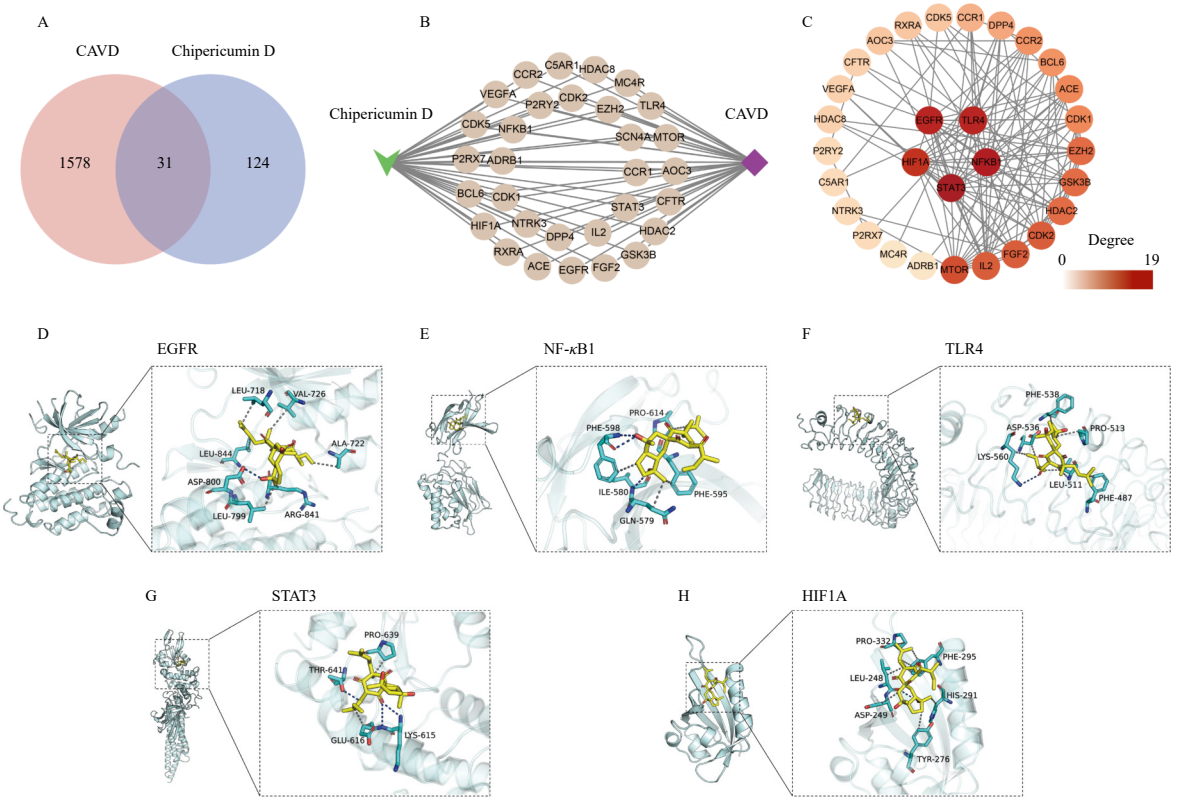

Fig. 4 Identification of potential targets of chipericumin D in CAVD. (A) Venn diagram showing the numbers of targets related to chipericumin D and CAVD. (B) Chipericumin D–CAVD target network, in which pale yellow indicates targets, purple indicates CAVD, and green indicates chipericumin D. (C) Protein–protein interaction (PPI) network of overlapping targets. Node color was scaled according to degree value, with redder nodes indicating higher degree values. (D) Molecular docking analysis of chipericumin D with EGFR, showing a hydrogen bond formed with Asp-800 in EGFR. (E) Chipericumin D forms hydrogen bonds with Ile-580 and Phe-598 in NF-κB1. (F) Chipericumin D forms hydrogen bonds with Lys-560 and Leu-511 in TLR4. (G) Chipericumin D forms hydrogen bonds with Lys-615, Thr-641, and Glu-616 in STAT3. (H) Chipericumin D forms a hydrogen bond with Leu-248 in HIF1A. The left panel presents the overall structure, whereas the right panel shows an enlarged view. Yellow sticks indicate the small molecule, cyan cartoons indicate the proteins, blue lines indicate hydrogen bonds, and gray dashed lines indicate hydrophobic interactions.

tiple sites contributed strong van der Waals forces.

3.6. Chipericumin D binds to the target of EGFR

To validate binding between chipericumin D and its predicted targets, we performed DARTS, CETSA, and SPR assays. First, we used the DARTS method *in vitro* [19], which relies on the resistance of target proteins to pronase E hydrolysis upon compound binding, resulting in differential band intensities on Western blots. Because pronase E hydrolysis reduces protein concentration, we quantified protein levels *via* BCA assay before terminating the reaction (Fig. 5A, Figs. S3A and S3H). We validated binding for targets with docking energies ≤ −6 kcal·mol^{-1}, namely EGFR, NF-κB1, TLR4, and STAT3. Binding between EGFR and chipericumin D *in vitro* was evident at 1000 μmol·L^{-1} chipericumin D and a pronase E-to-protein mass ratio of 1∶200 (Figs. S3B–S3G), whereas binding to other targets was minimal (Figs. S3B–S3G). Consistent results were obtained across a chipericumin D concentration gradient at the same protease ratio (Figs. S3I-S3N), confirming that under optimal conditions (1000 μmol·L^{-1} chipericumin D, 1:200 pronase E-to-protein ratio), DARTS corroborated prior findings (Figs. 5A–5C). Thus, EGFR is the most probable target.

Next, CETSA analysis assessed the chipericumin D-EGFR interaction. Treatment with chipericumin D (3 μmol·L^{-1}) reduced EGFR degradation across a temperature gradient (Figs. 5D–5E). Moreover, in hVICs treated with increasing chipericumin D concentrations for 24 h, EGFR degradation at 57 °C diminished with higher compound doses (Figs. 5F–5G). was conducted to further validate the interaction between chipericumin D and EGFR. Chipericumin D exhibited dose-dependent binding to EGFR, with a K_D of 5.11 μmol·L^{-1}, a K_a of 7.94 × 10^4 M^{-1}·s^{-1}, and a K_d of 0.406 s^{-1} (Fig. 5H). This K_D value indicates high binding affinity, suggesting formation of a stable chipericumin D-EGFR complex. Collectively, these results confirm that chipericumin D binds EGFR, supporting the molecular docking predictions.

3.7. GO analysis and KEGG pathway enrichment analyses

EGFR activates numerous downstream signaling pathways, including phosphatidylinositol 3-kinase (PI3K)-protein kinase B (AKT), Ras-Raf-MAPK, and JAK-STAT. Therefore, we conducted GO and KEGG enrichment analyses using the 31 overlapping targets identified earlier (Fig. 4A). Using the STRING database and applying a corrected *P*-value threshold of $P < 0.05$, the intersecting targets were enriched in 233 molecular functions, 2687 biological processes, and 130 cellular components (Fig. S5 and Table S3). Additionally, 174 signaling pathways were enriched, with significant KEGG pathway enrichment observed for EGFR and PI3K-AKT signaling (Fig. 6A and Table S3).

3.8. Chipericumin D inhibits hVIC osteogenic differentiation by disrupting the EGFR/PI3K/AKT signaling pathway

As established, EGFR is a direct target of chipericumin D. The PI3K-AKT pathway is significantly up-regulated in CAVD [24] and is activated downstream of EGFR signaling [25]. Furthermore, chipericumin D forms a hydrogen bond with EGFR at Asp-800 (Fig. 4D), a residue spatially proximal to Tyr1068, a well-characterized phosphorylation site essential for EGFR activation [26, 27]. Thus, we assessed phosphorylated (p)-EGFR, p-PI3K, and p-AKT protein levels in OM-treated hVICs as indicators of calcification. Chipericumin D effectively reversed OM-induced increases in p-EGFR, p-PI3K, and p-AKT (Figs. 6B–6E), although *EGFR* mRNA

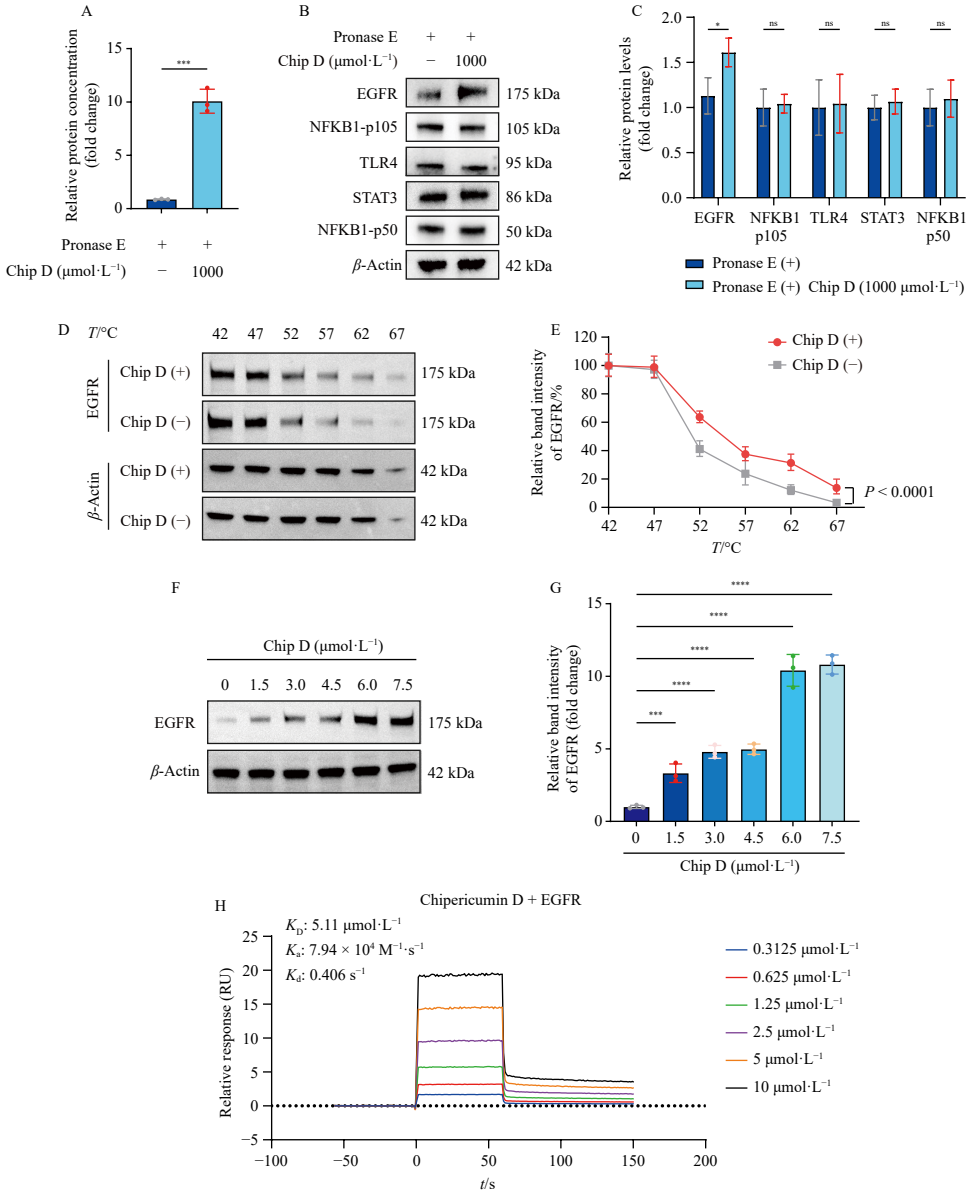

Fig. 5 Chipericumin D binds to the target of EGFR. (A) The results of drug affinity responsive target stability (DARTS) protein concentration based on chipericumin D (Chip D, 1000 μmol·L^{-1}) with pronase E (pronase E∶protein = 1∶200). (B–C) The western blotting of DARTS based on Chip D (1000 μmol·L^{-1}) with pronase E (pronase E∶protein = 1∶200) (D–E) Chip D (3 μmol·L^{-1}) enhances the thermal stability of EGFR in hVICs in a temperature-dependent manner, as determined by a cellular thermal shift assay (CETSA). (F–G) Chip D enhances the thermal stability of EGFR in hVICs in a dose-dependent manner at 57 °C, as determined by a CETSA. (H) Surface plasmon resonance (SPR) analysis of the interactions between Chip D and EGFR. Data are presented as means ± SD (n = 3). $^{*}P$ < 0.05 was considered a significant difference; $^{***}P$ <0.001, $^{****}P$ < 0.0001.

levels remained unchanged (Fig. 6F). IF staining further confirmed that chipericumin D significantly reduced p-EGFR levels (Figs. 6G–6H).

To confirm that chipericumin D modulates osteogenic differentiation *via* the EGFR/PI3K/AKT pathway, we conducted rescue experiments using the EGFR phosphorylation activator NSC 228155 and the AKT phosphorylation activator SC79. Consistent with prior results, chipericumin D significantly suppressed phosphorylation of EGFR and its downstream PI3K-AKT effectors (Figs. 7A–7F). NSC 228155 (100 nmol·L^{-1}) markedly enhanced EGFR and PI3K/AKT phosphorylation without altering total protein levels in OM-induced hVICs (Figs. 7A–7F). Similarly, SC79 (5 μmol·L^{-1}) reversed chipericumin D-mediated inhibition of AKT phosphorylation (Figs. S6A–S6D), further supporting the role of this pathway. AR and ALP staining confirmed that NSC 228155 or SC79 reversed the anti-osteogenic effects of chipericumin D (Figs. 7G–7I). In summary, chipericumin D inhibits hVIC osteogenic differentiation by interfering with the EGFR/PI3K/AKT signaling cascade.

4. Discussion

Dot-blotting has long been employed for semi-quantitative analysis of intracellular DNA/RNA levels [9]. Its advantages, including simplicity, speed, efficiency, and high-throughput capability, facilitate large-scale compound screening in CAVD. In our study, VICs were cultured in high-glucose (HG, 4.5 g·L^{-1}) DMEM, as glucose can promote VIC differentiation into osteoblast-like cells and up-regulate RUNX2 expression [28]. Critically, our OM formulation incorporated HG-DMEM, thereby maintaining a glucose-enriched, pro-osteogenic metabolic environment while providing additional stimuli that further enhanced VIC osteogenic differentiation and RUNX2 expression [28]. This dual-stimulation strategy established an optimized pathophysiological model for drug screening and mechanistic studies using dot-blotting.

Chipericumin D, isolated from *Hypericum monogynum* L. [23],

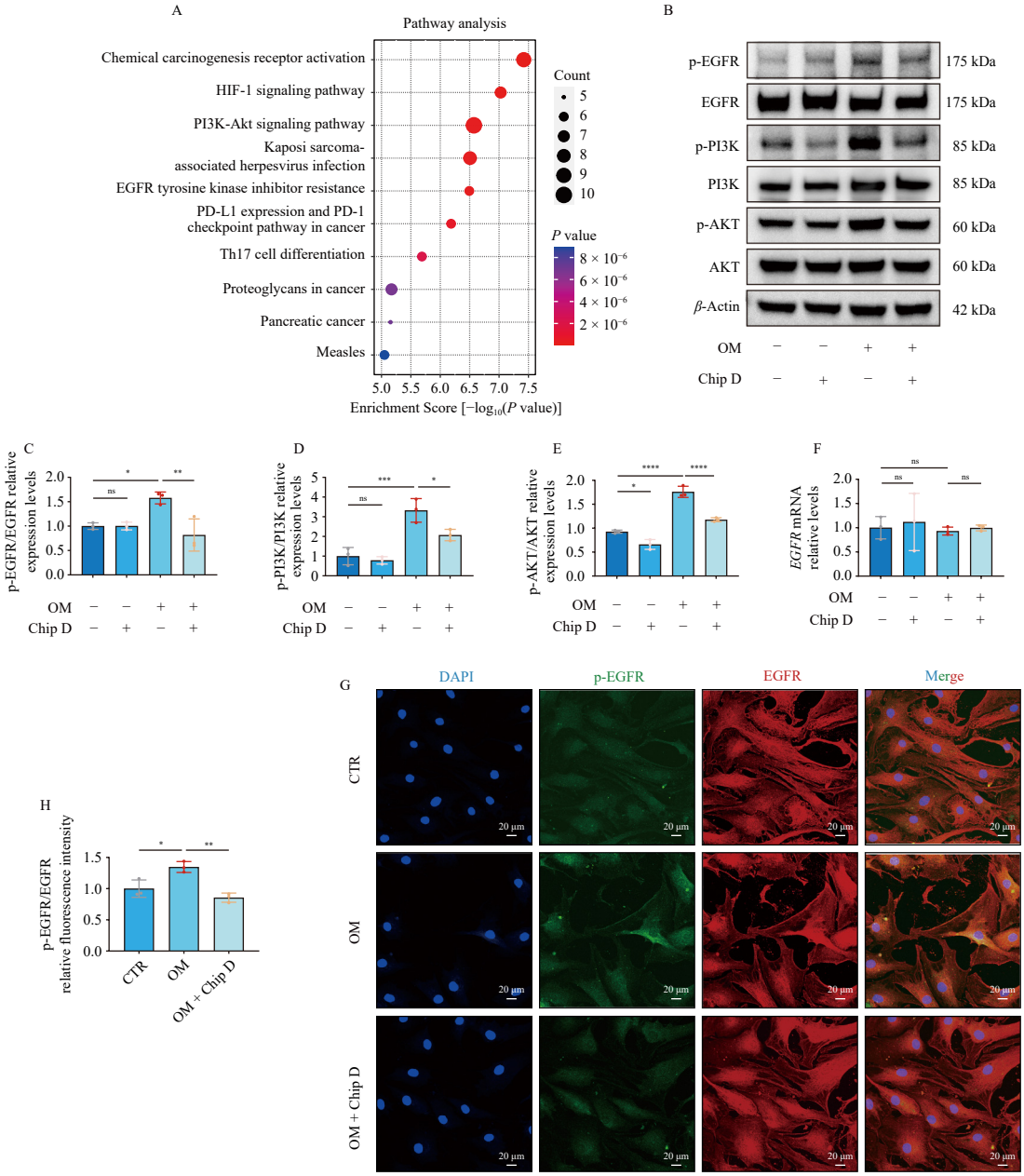

Fig. 6 Chipericumin D binds to EGFR and inhibits the EGFR/PI3K/AKT signaling pathway. (A) KEGG enrichment analysis of the 31 overlapping targets between CAVD and chipericumin D (Chip D). (B–E) Western blotting analysis of the protein expression levels of p-EGFR, EGFR, p-PI3K, PI3K, p-AKT, AKT. (F) *EGFR* mRNA expression levels. (G–H) Immunofluorescence staining of p-EGFR and EGFR (scale bar: 20 μm). Chip D (3 μmol·L^{-1}) was used for treatment. Data are presented as means ± SD (n = 3). $^{*}P < 0.05$ was considered a significant difference; $^{**}P < 0.01$, $^{***}P < 0.001$, $^{****}P < 0.0001$.

was identified as a candidate inhibitor of hVIC osteogenic differentiation through screening of our in-house compound library. Previous studies report that *Hypericum* [29] species constituents exhibit therapeutic potential in neurodegenerative diseases, cardiovascular disorders, and cancers [30]. However, the pharmacological effects of chipericumin D have not been previously investigated in any disease context.

Our results demonstrate that chipericumin D inhibits osteogenic differentiation in hVICs at 3 μmol·L^{-1}, a non-cytotoxic concentration. In contrast, effective concentrations of other anti-calcification agents such as curcumin [24] and caffeic acid phenethyl ester [31] are higher than that of chipericumin D. Thus, chipericumin D represents a promising candidate for CAVD treatment, with potentially lower toxicity.

PPI network analysis, molecular docking, DARTS, CETSA, and SPR collectively confirmed that chipericumin D binds to EGFR. Although multiple pathological targets have been implicated in CAVD, including proprotein convertase subtilisin/kexin type 9 (PCSK9) [9] and dipeptidyl peptidase 4 (DPP4) [32], the role of EGFR in CAVD remains poorly characterized. EGFR encodes a receptor tyrosine kinase that regulates cell survival, growth, proliferation, and differentiation [33]. Dysregulation of EGFR has been reported in various cancers [34, 35] and may [36] [36] activate downstream signaling pathways like PI3K-AKT [37] through tyrosine phosphorylation. Consequently, EGFR may strongly influence hVIC osteogenic differentiation [24]. Therefore, EGFR-targeted small molecules, siRNAs, or viral vectors may offer novel therapeutic strategies for CAVD.

KEGG enrichment analysis revealed that the 31 overlapping targets of chipericumin D and CAVD were significantly enriched in EGFR and PI3K-AKT signaling pathways. Chipericumin D forms a hydrogen bond with EGFR at Asp-800 (Fig. 4D), near the phosphorylation site Tyr1068 [26, 27]. We observed elevated p-EGFR under OM induction, which decreased upon chipericumin D treatment. Rescue experiments demonstrated that EGFR or AKT agonists restored pathway activity suppressed by chipericumin D.

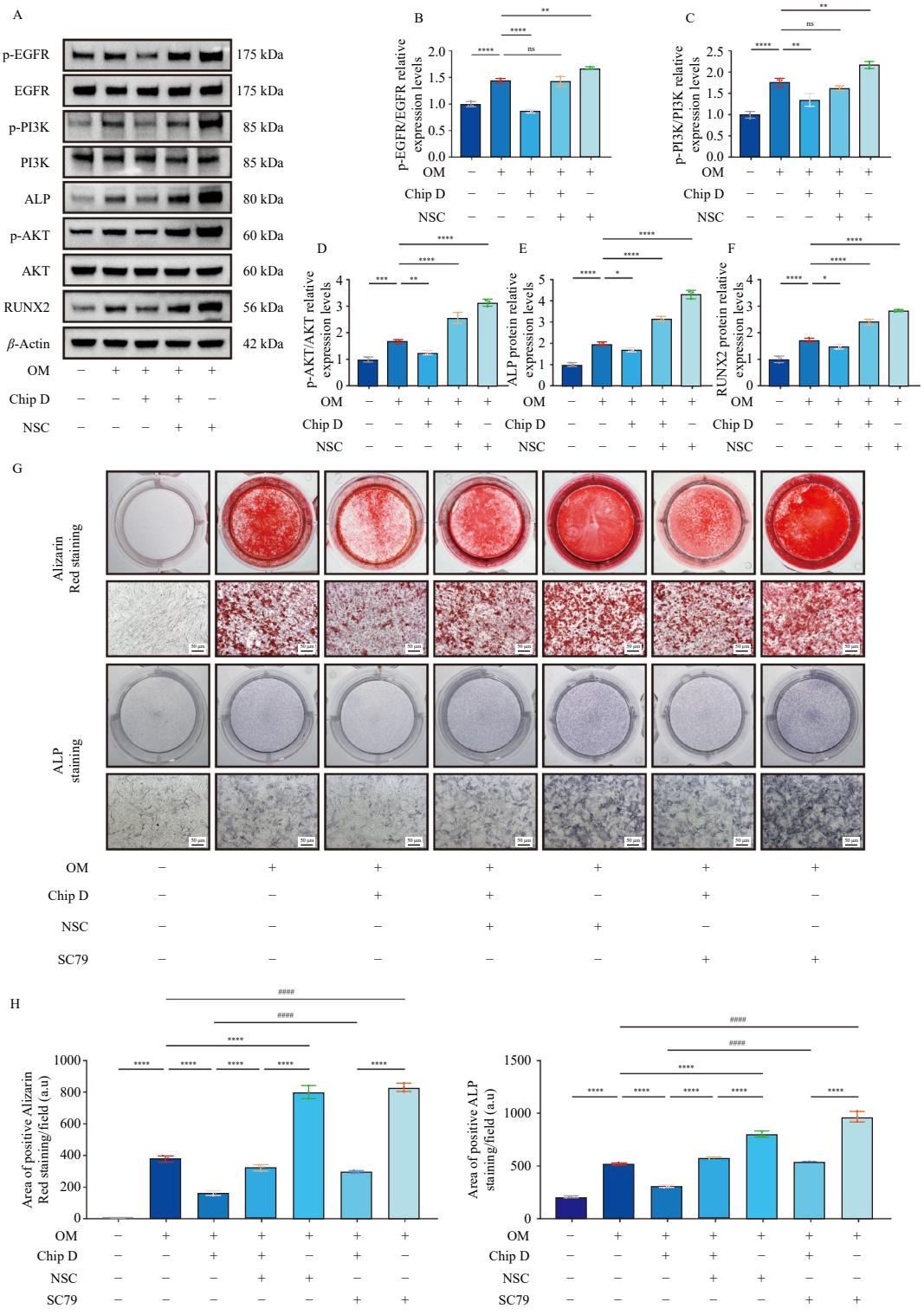

Fig. 7 Chipericumin D inhibits the osteogenic differentiation of hVICs by interfering with the EGFR/PI3K/AKT signaling pathway. (A–F) Western blotting analysis of hVICs ubjected to different treatments, including NSC 228155 (100 nmol·L^{-1}), Chip D (3 μmol·L^{-1}), and SC79 (5 μmol·L^{-1}). (G–I) Alizarin Red staining (OM for 21 days) and ALP staining (OM for 7 days) of hVICs subjected to different treatments, including NSC 228155 (100 nmol·L^{-1}), Chip D (3 μmol·L^{-1}), and SC79 (5 μmol·L^{-1}). Data are presented as means ± SD (n = 3). $^{*}P < 0.05$ and $^{\#}P < 0.05$ were considered statistically significant; $^{**}P < 0.01$, $^{***}P < 0.001$, ****, $^{\#\#\#\#}P < 0.0001$.

These findings indicate that chipericumin D modulates hVIC osteogenic differentiation by inhibiting EGFR phosphorylation. Future work will validate the pharmacological effects of chipericumin D *in vivo* to assess its potential for drug development.

5. Conclusion

In summary, our findings demonstrate that chipericumin D inhibits osteogenic differentiation of hVICs by interfering with EGFR phosphorylation and subsequent activation of the EGFR/PI3K/AKT signaling pathway (Fig. 8). Thus, chipericumin D holds promise as a therapeutic agent for preventing or treating CAVD, and our data provide preliminary evidence that EGFR is a novel therapeutic target for this disease.

Ethics statement

The aortic valves were derived from patients who under-

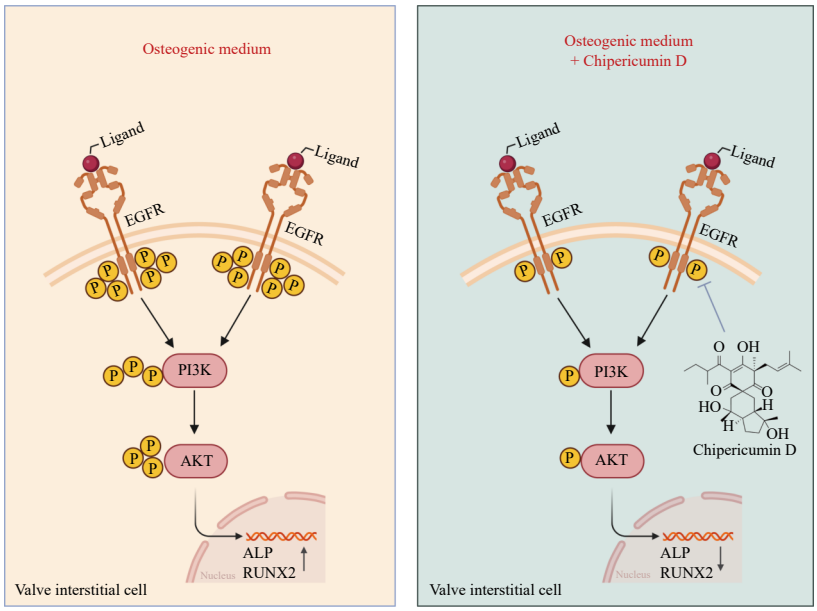

Fig. 8 Diagram of chipericumin D inhibits osteogenic differentiation of hVICs by affecting the activation of the EGFR/PI3K/AKT signaling pathway. Created with BioRender.com.

went Bentall surgery in the Department of Cardiovascular Surgery, Union Hospital, Tongji Medical College, Huazhong University of Science and Technology. The Review Board of Union Hospital, Tongji Medical College, Huazhong University of Science and Technology (Approval #20230278) authorized all human experiments, and written consent was obtained from every participant.

Funding

This work was supported by the National Key R&D Program of China (Nos. 2021YFA1101900 and 2021YFA0910500), the National Natural Science Foundation of China (Nos. 82100303, 82273811, 22577033, 82470423, and 82404822), the Hubei Provincial Natural Science Foundation Projects (Nos. JCZRYB2025-00142 and 2024AFA028), the Wuhan International Science and Technology Cooperation Project (No. 2025071204030392), the Fundamental Research Funds for the Central Universities (HUST: Nos. YCJJ20252429 and 2025BRA015), the National Program for Support of Top-notch Young Professionals (No. 0106514050), the Guangdong Basic and Applied Basic Research Foundation (No. 2023A1515110763), the China Postdoctoral Science Foundation (No. 2023M742415), the Shenzhen Science and Technology Program (No. JCYJ20220818101806014), and the Team-based Medical Science Research Program (No. 2024YZZ11).

Supporting information

Supplementary data associated with this article can berequested by sending E-mail to the corresponding authors.

Declaration of competing interest

These authors declare no conflict of interest.

Acknowledgment

Thanks for the technical support by the Medical Subcenter of HUST Analytical & Testing Center.

Declaration of generative AI and AI-assisted technologies in the writing process

In the writing process, we used GPT-3.5 for language translation. Additionally, we affirm that we did not rely on Generative AI or AI-assisted technologies to generate any original thoughts or content, and we thoroughly reviewed the article and take complete responsibility for its content.

References

1 Yi B, Zeng WK, Lv L, et al. Changing epidemiology of calcific aortic valve disease: 30-year trends of incidence, prevalence, and deaths across 204 countries and territories. *Aging (Albany NY)*. 2021;13(9):12710-12732. https://doi.org/10.18632/aging.202942.
2 Roth GA, Mensah GA, Johnson CO, et al. Global burden of cardiovascular diseases and risk factors, 1990-2019: update from the GBD 2019 study. *J Am Coll Cardiol*. 2020;76(25):2982-3021. https://doi.org/10.1016/j.jacc.2020.11.010.
3 Vahanian A, Beyersdorf F, Praz F, et al. 2021 ESC/EACTS Guidelines for the management of valvular heart disease. *Eur Heart J*. 2022;43(7):561-632. https://doi.org/10.1093/eurheartj/ehab395.
4 Makkar RR, Thourani VH, Mack MJ, et al. Five-year outcomes of transcatheter or surgical aortic-valve replacement. *N Engl J Med*. 2020;382(9):799-809. https://doi.org/10.1056/NEJMoa1910555.
5 Witberg G, Codner P, Landes U, et al. Effect of transcatheter aortic valve replacement on concomitant mitral regurgitation and its impact on mortality. *JACC Cardiovasc Interv*. 2021;14(11):1181-1192. https://doi.org/10.1016/j.jcin.2021.02.030.
6 Lee G, Chikwe J, Milojevic M, et al. ESC/EACTS *vs* ACC/AHA guidelines for the management of severe aortic stenosis. *Eur Heart J*. 2023;44(10):796-812. https://doi.org/10.1093/eurheartj/ehac803.
7 Chan KL, Teo K, Dumesnil JG, et al. Effect of lipid lowering with rosuvastatin on progression of aortic stenosis: results of the aortic stenosis progression observation: measuring effects of rosuvastatin (ASTRONOMER) trial. *Circulation*. 2010;121(2):306-314. https://doi.org/10.1161/circulationaha.109.900027.
8 Qian XY, Xu L, Geng BC, et al. Navigating the landscape of translational medicine of calcific aortic valve disease: bridging bench to bedside. *JACC Asia*. 2025;5(4):503-515. https://doi.org/10.1016/j.jacasi.2025.01.014.
9 Han D, Zhou TW, Li LF, et al. AVCAPIR: a novel procalcific PIWI-interacting RNA in calcific aortic valve disease. *Circulation*. 2024;149(20):1578-1597. https://doi.org/10.1161/circulationaha.123.065213.
10 Liu ZT, Wang K, Jiang C, et al. Morusin alleviates aortic valve calcification by inhibiting valve interstitial cell senescence through Ccnd1/Trim25/Nrf2 axis. *Adv Sci (Weinh)*. 2024;11(20):e2307319. https://doi.org/10.1002/advs.202307319.
11 Liu ZT, Wang YX, Liu FY, et al. Long noncoding TSI attenuates aortic valve calcification by suppressing TGF-β1-induced osteoblastic differentiation of valve interstitial cells. *Metabolism*. 2023;138:155337. https://doi.org/10.1016/j.metabol.2022.155337.
12 Rutkovskiy A, Malashicheva A, Sullivan G, et al. Valve interstitial cells: the key to understanding the pathophysiology of heart valve calcification. *J Am Heart Assoc*. 2017;6(9):e006339. https://doi.org/10.1161/jaha.117.006339.
13 Moncla LM, Briend M, Bossé Y, et al. Calcific aortic valve disease: mechanisms, prevention and treatment. *Nat Rev Cardiol*. 2023;20(8):546-559. https://doi.org/10.1038/s41569-023-00845-7.
14 Theodoris CV, Zhou P, Liu L, et al. Network-based screen in iPSC-derived cells reveals therapeutic candidate for heart valve disease. *Science*. 2021;371(6530):eabd0724. https://doi.org/10.1126/science.abd0724.

15 Yang J, Grafton F, Ranjbarvaziri S, et al. Phenotypic screening with deep learning identifies HDAC6 inhibitors as cardioprotective in a BAG3 mouse model of dilated cardiomyopathy. *Sci Transl Med*. 2022;14(652):eabl5654. https://doi.org/10.1126/scitranslmed.abl5654.
16 Jiang C, Yao DY, Liu ZT, et al. FOXO1 regulates RUNX2 ubiquitination through SMURF2 in calcific aortic valve disease. *Redox Biol*. 2024;73:103215. https://doi.org/10.1016/j.redox.2024.103215.
17 Geng BC, Chen X, Chi JY, et al. Platelet membrane-coated alterbrassicene A nanoparticle inhibits calcification of the aortic valve by suppressing phosphorylation P65 NF-κB. *Theranostics*. 2023;13:3781-3793. https://doi.org/10.7150/thno.85323.
18 Moumbock AFA, Li J, Tran HTT, et al. ePharmaLib: a versatile library of e-pharmacophores to address small-molecule (poly-)pharmacology. *J Chem Inf Model*. 2021;61(7):3659-3666. https://doi.org/10.1021/acs.jcim.1c00135.
19 Ren YS, Li HL, Piao XH, et al. Drug affinity responsive target stability (DARTS) accelerated small molecules target discovery: principles and application. *Biochem Pharmacol*. 2021;194:114798. https://doi.org/10.1016/j.bcp.2021.114798.
20 Ye WL, Yang PL, Jin M, et al. Dihydromyricetin mitigates abdominal aortic aneurysm *via* transcriptional and post-transcriptional regulation of heme oxygenase-1 in vascular smooth muscle cells. *Acta Pharm Sin B*. 2025;15(3):1514-1534. https://doi.org/10.1016/j.apsb.2025.02.003.
21 Yang Z, Wang W, Qi Y, et al. Exploring new catechin derivatives as SARS-CoV-2 M^{pro} inhibitors from tea by molecular networking, surface plasma resonance, enzyme inhibition, induced fit docking, and metadynamics simulations. *Comput Biol Med*. 2022;151(Pt A):106288. https://doi.org/10.1016/j.compbiomed.2022.106288.
22 Olaru A, Bala C, Jaffrezic-Renault N, et al. Surface plasmon resonance (SPR) biosensors in pharmaceutical analysis. *Crit Rev Anal Chem*. 2015;45(2):97-105. https://doi.org/10.1080/10408347.2014.881250.
23 Abe S, Tanaka N, Kobayashi J. Prenylated acylphloroglucinols, chipericumins A–D, from *Hypericum chinense*. *J Nat Prod*. 2012;75(3):484-488. https://doi.org/10.1021/np200741x.
24 Zhou TW, Wang YJ, Liu M, et al. Curcumin inhibits calcification of human aortic valve interstitial cells by interfering NF-κB, AKT, and ERK pathways. *Phytother Res*. 2020;34(8):2074-2081. https://doi.org/10.1002/ptr.6674.
25 Huang LH, Fu LW. Mechanisms of resistance to EGFR tyrosine kinase inhibitors. *Acta Pharm Sin B*. 2015;5(5):390-401. https://doi.org/10.1016/j.apsb.2015.07.001.
26 He J, Wong LY, Chen S, et al. Inhibition of the PI3K/AKT signaling pathway contributes to the anti-renal cell carcinoma effects of deoxyelephantopin. *Biomed Pharmacother*. 2025;187:118136. https://doi.org/10.1016/j.biopha.2025.118136.
27 Li Y, Chen JY, Liang HJ, et al. Gasdermin D regulates the activation of EGFR in colorectal cancer. *J Transl Med*. 2024;22(1):1170. https://doi.org/10.1186/s12967-024-05984-0.
28 Voicu G, Rebleanu D, Constantinescu CA, et al. Nano-polyplexes mediated transfection of Runx2-shRNA mitigates the osteodifferentiation of human valvular interstitial cells. *Pharmaceutics*. 2020;2(6):507. https://doi.org/10.3390/pharmaceutics12060507.
29 Sarikurkcu C, Locatelli M, Tartaglia A, et al. Enzyme and biological activities of the water extracts from the plants *Aesculus hippocastanum*, *Olea europaea* and *Hypericum perforatum* that are used as folk remedies in Turkey. *Molecules*. 2020;25(5):1202. https://doi.org/10.3390/molecules25051202.
30 Xia J, Wan Y, Wu JJ, et al. Therapeutic potential of dietary flavonoid hyperoside against non-communicable diseases: targeting underlying properties of diseases. *Crit Rev Food Sci Nutr*. 2024;64(5):1340-1370. https://doi.org/10.1080/10408398.2022.2115457.
31 Liu M, Li F, Huang YM, et al. Caffeic acid phenethyl ester ameliorates calcification by inhibiting activation of the AKT/NF-κB/NLRP3 inflammasome pathway in human aortic valve interstitial cells. *Front Pharmacol*. 2020;11:826. https://doi.org/10.3389/fphar.2020.00826.
32 Wang YY, Han D, Zhou TW, et al. DUSP26 induces aortic valve calcification by antagonizing MDM2-mediated ubiquitination of DPP4 in human valvular interstitial cells. *Eur Heart J*. 2021;42(30):2935-2951. https://doi.org/10.1093/eurheartj/ehab316.
33 Zubair T, Bandyopadhyay D. Small molecule EGFR inhibitors as anti-cancer agents: discovery, mechanisms of action, and opportunities. *Int J Mol Sci*. 2023;24(3):2651. https://doi.org/10.3390/ijms24032651.
34 Harrison PT, Vyse S, Huang PH. Rare epidermal growth factor receptor (EGFR) mutations in non-small cell lung cancer. *Semin Cancer Biol*. 2020;61:167-179. https://doi.org/10.1016/j.semcancer.2019.09.015.
35 Napolitano S, Martini G, Ciardiello D, et al. Targeting the EGFR signalling pathway in metastatic colorectal cancer. *Lancet Gastroenterol Hepatol*. 2024;9(7):664-676. https://doi.org/10.1016/s2468-1253(23)00479-x.
36 Levantini E, Maroni G, Del Re M, et al. EGFR signaling pathway as therapeutic target in human cancers. *Semin Cancer Biol*. 2022;85:253-275. https://doi.org/10.1016/j.semcancer.2022.04.002.
37 Ganesan K, Xu C, Wu JM, et al. Ononin inhibits triple-negative breast cancer lung metastasis by targeting the EGFR-mediated PI3K/Akt/mTOR pathway. *Sci China Life Sci*. 202467(9):1849-1866. https://doi.org/10.1007/s11427-023-2499-2.